Construction and Building Materials 489 (2025) 142282

Contents lists available at ScienceDirect

Construction and Building Materials

journal homepage: www.elsevier.com/locate/conbuildmat

Influence of limestone addition on the engineering and durability performance of Portland-blast furnace slag blended concretes

Moro Sabtiwu [a,*], Yuvaraj Dhandapani [a,b], Michal P. Drewniok [a], Samuel Adu-Amankwah [a,c], Susan A. Bernal [a,d,**]

[a] School of Civil Engineering, University of Leeds, Woodhouse Lane, Leeds LS29JT, United Kingdom
[b] Institute of Functional Surfaces, School of Mechanical Engineering, University of Leeds, Woodhouse Lane, Leeds LS29JT, United Kingdom
[c] School of Engineering and Applied Science, Aston University, Birmingham B4 7ET, United Kingdom
[d] Department of Architecture and Civil Engineering, University of Bath, Claverton Down, Bath BA2 7AY, United Kingdom

ARTICLE INFO

Keywords:
CEM VI
Composite cements
Limestone-slag blended cements
Compressive Strength
Flexural Strength
Elasticity Modulus
Poisson ratio
Resistivity
Water permeability
Chloride migration

ABSTRACT

The widespread use of ternary cement produced from Portland cement (CEM I), granulated blast furnace slag (GGBFS) and limestone powder in structural concrete can be anticipated given the recent standardisation of such ternary cements in EN 197–5. However, understanding of these cements is limited to paste or mortar-scale studies, and comprehensive studies on concretes produced from such cements are needed urgently. In this study, fresh and hardened properties including strength, elastic modulus, water absorption and chloride permeability of ternary cement concrete comprising 50 wt% CEM I blended with GGBFS and 10 or 20 wt% limestone are investigated, as a function of the curing duration. Reducing the GGBFS content, by replacing it with 10–20 wt% limestone powder, leads to satisfactory mechanical and durability properties relative to binary and CEM I concrete. It was established that the ternary concretes evaluated exhibit a progressive increase in compressive strength, reaching values comparable to those of the reference CEM I concrete by 365 days of curing. The flexural strength, static and dynamic elastic moduli of the GGBFS-containing concretes, with or without limestone, are comparable to CEM I concrete, at the investigated curing ages. The chloride permeability and water sorption studies demonstrated that concrete made of composite cements containing up to 20 wt% limestone has no detrimental implications on the resistance to chlorides and water ingress. This study also demonstrates that the mechanical properties of concretes with high replacement of blast furnace slag in Portland blended cements, with or without limestone, are compliant with ACI, *fib* and Eurocode 2 for structural concrete applications.

1. Introduction

Reducing the clinker factor is one of the key strategies adopted by the cement and concrete industries to reduce the carbon footprint of the construction sector, and to meet net zero targets [1,2]. This is achieved by using cement replacements or supplementary cementitious materials (SCMs), and/or limestone. Although the use of SCMs for the production of blended Portland cements is a well-established practice, in some regions, conventional SCMs such as fly ash or granulated blast furnace slag (referred to as GGBFS or slag in this manuscript) are becoming scarce, motivating the use of other highly abundant cement replacements such as limestone instead [3]. Also, in several regions Portland limestone cements (PLC in North America [4] or CEM II/A-L in Europe [5]) are becoming the prevalent cement type being commercialised. PLC or CEM II/AL cements with moderated levels (10–15 wt%) of limestone powder have been extensively utilised as efficient alternatives to Portland cement (OPC or CEM I) with similar performance [6,7]. More recently, multicomponent binders with reduced clinker contents are being adopted, which compromise OPC clinker, a SCM and limestone powder, and often referred to as composite cements [8]. These binders have recently been included in various cement and concrete standards (BS 8500–2:2023 [9] and the EN 197–5:2021 [8]) enabling its use in concrete production.

It has been extensively studied [10–13] the synergistic benefit of

* Corresponding author.
** Corresponding author at: Department of Architecture and Civil Engineering, University of Bath, Claverton Down, Bath BA2 7AY, United Kingdom.
E-mail address: Sbl30@bath.ac.uk (S.A. Bernal).

https://doi.org/10.1016/j.conbuildmat.2025.142282
Received 13 December 2024; Received in revised form 13 May 2025; Accepted 12 June 2025
Available online 17 June 2025

limestone addition in the improvement of hydration kinetics of clinker and/or slag hydration through the provision of additional nucleation sites, as well as its influence on microstructure related properties. The reaction of limestone with tricalcium aluminate yields mono-carboaluminates formation, which stabilises ettringite [14,15] and further contributes to increasing the solid volume due to the low density of ettringite phase compared to other hydration products. In ternary slag systems, limestone addition favours slag dissolution enhancing clinker hydration [13], thus facilitating accelerated hydration, limiting the early age retarding effect of slag hydration by high alumina concentrations in the pore water upon its dissolution [10]. It has also been reported [16] that in ternary systems, using different slag to limestone ratios had a minimal effect of the total heat of reaction, consistent with the results from [10], however, higher limestone content led to improved porosity and expedited the reaction kinetics. Since composite ternary binder contain multiple ingredients, the specific surface of each component is also important. Adu-Amankwah et al. [17] identified that the fineness of CEM I, GGBFS and limestone can be optimised to maximise reactivity of composite cements, and increasing fineness does not necessarily lead to higher reaction degree. Equally the blending method (intergrinding or interblended) could also influence hydration kinetics and mechanical performance due to differences in grinding efficiency of different ingredients in ternary cement [18]. This means that in composite cements, the optimised specific surface of each component as a function of their chemistry can facilitate the use of lower clinker content for a comparable reaction kinetics and strength development.

The main hydration products in ternary slag-limestone systems, as predicted by GEMS thermodynamic modelling and extensively verified by experimental evidence, are an aluminium substituted calcium silicate hydrate (C-(A)-S-H type gel, portlandite, carboaluminates and hydrogarnets [14,19,20]. The synergetic effect of limestone with the Portland cement and blast furnace slag, leads to pore filling due to additional hydrates formation which in turns leads to a refined pore structure, which impacts the strength development and durability properties [10, 21]. However, the implications of changes in reaction kinetics and phase assemblages of ternary slag-limestone cements on the mechanical and durability performance when used for structural concrete production is not widely reported, particularly in cognisance with design codes. Evaluation of the performances of composite cement concrete is necessary to accelerate the adoption of these binders in construction practices, including determining the applicability of existing design codes and standards, which is the main objective of the present study.

Addition of limestone powder has been reported to influence the fresh properties of concretes in both binary and ternary mixtures. Limestone addition in low dosages (<10–20 wt%) to Portland clinker can enhance workability of fresh concrete; however, increasing the limestone content above 20 wt% reduces workability and concrete mixes necessitate the addition of a superplasticizer [22,23]. Besides particle size and specific surface area (SSA) of limestone, morphology and purity of limestone can also affect the fresh properties of concrete mixes [24]. There is also a growing interest to explore the use of low purity limestone [25] from cement quarries that are not suitable for cement production which would also modify the phase assemblage and early age performance in composite systems containing limestone [18, 26,27].

It has been reported that, for a similar water-binder-ratio, concretes made from ternary Portland-slag-limestone with ~20 wt% limestone addition exhibited comparable strengths to binary slag and CEM I concrete [28,29]. The use of multicomponent composite cements can lead to variation in fresh and hardened properties of a concrete mixture depending on the blend compositions, limestone replacement level and choice of SCM used. A few reports exist evaluating the influence of low levels of limestone addition (<10 wt%) in the performance Portland concrete, particularly in-service conditions [30,31]. Since composite cements, also referred to as CEM VI cement, with high volume replacement of Portland cement with slag and limestone have only recently been included in European standards, these materials lack of an in-service track record. Consequently, their longer-term durability performance can be perceived as one of the barriers to limit their widespread use. There are limited studies in the literature on concrete produced with ternary Portland-blast furnace slag- limestone cements with existing studies focusing on compressive strength and early age durability testing in concrete [28,29,32].

Durability of blast furnace slag blended Portland concretes is well documented [33–35], highlighting the potential beneficial role of high volume slag based concrete on pore structure [36] and resistance to chloride ingress in marine and other aggressive environments [37–39]. However, there is still limited understanding on the effect of the partial replacement of slag by limestone on the engineering of these composite concretes. The majority of studies on slag-limestone combination focuses on blend optimisation and hydration characteristics evaluated in paste specimens [10,11,40], with limited studies focusing on evaluating concrete specifically on transport properties and durability performance [41]. The present study aims to contribute to resolve this knowledge gap, to create the confidence for practitioners to adopt these materials in construction practices, and to identify their suitability for different exposure classes considered in the standards. This is essential for the widespread acceptance of composite cement type for structural concrete applications. The adoption of composite cements has the potential to alleviate future demand constrains as the availability of blast furnace slag is limited in many parts of world, enabling its most efficient use [42]. This, if similar performance can be attained by composite cement concrete to those reported in binary concrete.

This study reports the mechanical and durability aspects of sustainable concretes made with CEM I and slag-blended composite cements with or without limestone (up to 20 wt%). The mechanical properties tested included compressive strength, flexural strength, static elastic modulus, and UPV dynamic elastic modulus. The compliance of existing standards of slag-limestone composite concrete is also evaluated and discussed. Studies on the transport properties focused on moisture ingress (sorptivity and total water absorption), chloride permeability, as well as bulk conductivity and surface resistivity are conducted to determine the durability of these composite concretes. The results reported here will facilitate the adoption of slag-limestone composite concrete in construction practices, promoting the efficient use of blast furnace slag by co-substitution along with limestone to produce sustainable concrete.

2. Experimental methods

2.1. Materials

In this study, a CEM I 52.5 N and granulated blast furnace slag (GGBFS), were used as main binders. These materials were supplied by Heidelberg Materials UK, from Ribblesdale and Port Talbot works respectively. A limestone powder (conforms to BS 7979 [43]) supplied by LKAB minerals UK was used, as well as natural anhydrite supplied by Heidelberg Materials UK. Table 1 shows the oxide compositions of the materials used in this study, determined by X-ray fluorescence (XRF) spectroscopy using a Rigaku ZSX Primus II, with the fused bead preparation method. The quality ($CaO + Al_2O_3 + MgO$ / $TiO_2 + SiO_2$) and basicity ($CaO + MgO$ /$Al_2O_3 + SiO_2$) coefficients of the slag used are 1.65 and 1.02 respectively. Based on laser granulometry (measured with a Malvern Mastersizer 2000 laser diffractometer, using a dry dispersion unit), the dry particle size distribution of CEM I, GGBFS and limestone are shown in Fig. 1(a), which present a d_{50} of 17.1 μm, 14.1 μm and 11.9 μm respectively. Density measurements based on helium pycnometry revealed values of 3136.4, 2917.3 and 2727.7 kg/m^3 for CEM I, GGBFS and limestone correspondingly. Limestone exhibited a bimodal particle size distribution, which is likely due to break up of large particles. Nitrogen adsorption-desorption measurements were conducted at

Table 1
Oxide compositions of CEM slag, limestone and anhydrite.

	Al_2O_3	SiO_2	CaO	SO_3	K_2O	Na_2O	MgO	TiO_2	MnO	Fe_2O_3	Trace	LOI*
CEM I	4.51	18.6	62.59	5.72	0.31	0.18	2.39	0.22	0.06	2.08	0.39	2.95
Slag	11.52	35.56	40.25	2.41	0.5	0.3	7.98	0.57	0.2	0.31	0. 41	-
Limestone	0.27	0.94	55.82	0.09	0.03	0.2	0.69	-	-	0.06	0.09	41.8
Anhydrite	0.8	2.37	38.35	52.18	0.19	0.34	1.4	-	-	0.25	0.34	3.8

* Loss on ignition (LOI) determined by wt. (%) change at room temperature and weight after 2hrs heating at 900 °C and ambient cooling

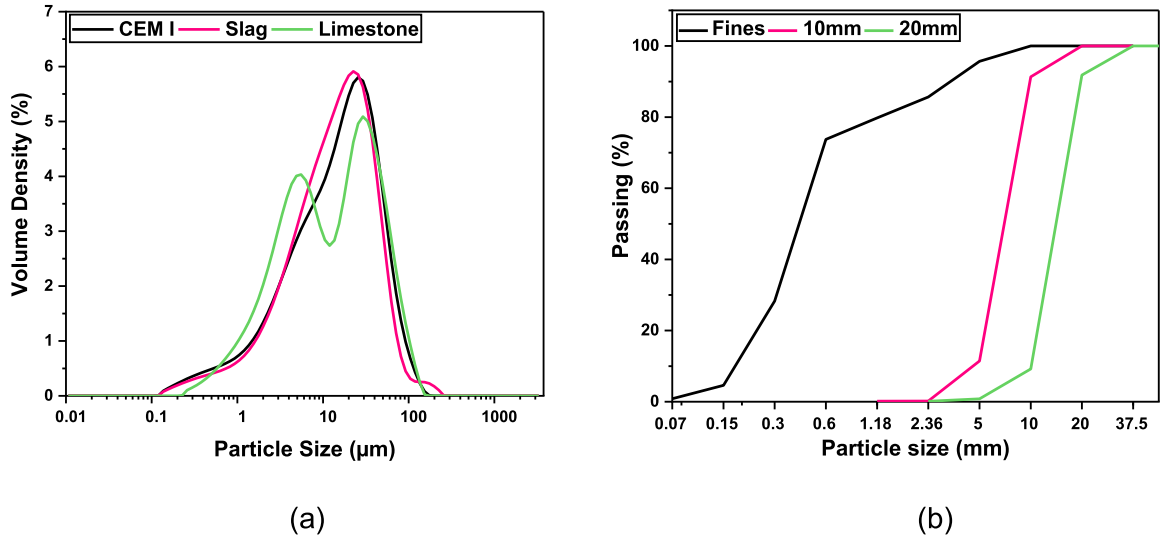

Fig. 1. (a) Particle size distribution determined by laser diffractometry of CEM I, GGBFS and limestone powders; and (b) Particle size distribution of aggregates as determined by sieving analysis.

77 K using a Micromeritics Tristar 3000 to ascertain the Brunauer-Emmett-Teller (BET) surface area. The BET specific surface of the materials used were 1.38 m^2/g for GGBS, 1.29 m^2/g for CEM I and 1.04 m^2/g for limestone.

The cementitious fraction was formulated to achieve ≥ 50 wt% CEM I replacement as shown in Table 2. The aggregates used for concrete production were uncrushed quartzite. The particle size distribution of sand and aggregates (max. size 10 mm and 20 mm) used for concrete production are shown in Fig. 1(b). The water absorption of sand, 10 mm and 20 mm aggregates was determined according to BS EN 1097–6:2022 (18) and the values for the different aggregate fractions were 1.9 (sand), 1.2 (10 mm aggregate) and 1.1 (20 mm aggregate) % respectively. Water corrections due to aggregates water absorption were factored in the concrete mix designs.

2.2. Concrete mix design and mixing

The mix designs used for producing concrete in this study are shown in Table 2. The binder content for all the concrete assessed was maintained at 320.3 kg/m^3 which conforms to the limiting values of concrete composition as prescribed by BS EN 206–2021 [in Table F.1 of the standard] [44] suitable for carbonation induced corrosion (XC1–4) and chlorides exposure classes XS(1−2) and XD(1−3). The mix design was developed on volumetric basis, so that cement/binder content as well as the ratio of water-to-binder was kept constant at 0.5, with additional approximate volumes apportioned to the aggregates. An air content of 2.5 % was targeted for the mixes. No air entrainment and super-plasticisers were used.

Dry aggregates and binder constituents were transferred into a planetary mixer and homogenised for 5 min, then water was added, and the concrete further mixed for another 5 min. The fresh properties of the concretes were immediately determined, followed by casting concrete specimens in plastic/metallic moulds as per BS EN 12390-2:2019 [45], and demoulded after 24 hrs, followed by storing in a curing room at 95 % relative humidity (RH) and 20 ± 3°C until testing.

2.3. Concrete characterisation

2.3.1. Fresh state properties

In this study, the slump test was conducted as per BS EN 12350–2:2019 [46]. The flow or spread of the concretes were measured based on BS EN 12350–5:2019 [47]. The BS EN 12390–7:2019 [48] standard was adopted for air content determination. The density of fresh concrete was determined in accordance with BS EN 12350–6:2019 [48].

Table 2
Concrete mix design (kg/m^3 of fresh mix).

Mix ID	CEM I 52.5 N	Slag	Limestone	Anhydrite	Water	Sand	10 mm Aggregates	20 mm Aggregates
N	320.3	-	-	-	160.2	651.8	237.7	950.8
NS	164.0	155.4	-	0.8	160.2	648.8	236.6	946.5
NSL	165.6	125.6	28.3	0.8	160.2	648.2	236.4	945.5
NS2L	167.2	93.2	59.0	0.8	160.2	647.5	236.1	944.5

*Note: In NS, NSL and NS2L mixes limestone and anhydrite are counted as part of the binder

2.3.2. Compressive and flexural strength testing

The compressive strength evolution of concrete mixes was determined at 2, 7, 28, 90,180 and 365 days of curing. Compression test was conducted at 6 kN/s loading rate on 100 mm cubes in triplicates in accordance with BS EN 12390–3:2019 [49], using a 3000 kN capacity MATEST crusher. The flexural strength of concretes was determined using the bending testing on duplicate 100 × 100 × 400 mm prismatic specimens, tested as 0.2 kN/s as per BS EN 12390–5:2019 [50].

2.3.3. Static elastic modulus and Poisson ratio determination

The static elastic modulus and the Poisson ratio of the concretes mixes was determined in accordance with the ASTM C469/C469M-22 [51] standard on two Ø100 × 200 mm cylinders per mix. Here, surface-dried concrete specimens were bonded with 60 mm, 120 Ω Tokyo instrument-supplied strain gauges using a hardened TEROSON UP 130 (mixed with benzoyl peroxide (BPO) paste) as substrate. The strain gauge length is dependent on largest aggregate in the concrete mixes. Before attaching strain gauges, the hardened TEROSON UP-130 was grounded with successive grades of sandpaper to achieve a smoothened and flattened surface, and the gauges were held in place with quick-drying glue.

Each cylinder was appended with four 120 Ω resistor strain gauges so that, two were positioned axially on the circumference at the mid-span of the cylinders in a diametrically parallel manner, and the other two strain gauges were placed laterally along the mid-height so that they are opposite to each other. The strain gauges were lead-soldered to wires, which were further connected to separate channels, each in a quarter-bridge circuit configuration attached to a Campbell® Scientific CR3000 micro logger. The data logger was connected to a computer program for strain data monitoring and collection, while a USB was used to download data on applied load (kN) to failure. The axial and lateral strain evolution of the cylinders were recorded when subjected to compressive loads to failure using the MATEST crusher at a loading rate of 3kN/s.

$$E_{st} = [S_2 - S_1]/(\varepsilon_2 - 0.00005) \quad (1)$$

Where:

S_1 = stress corresponding to longitudinal strain, ε1, of 50 millionths, MPa; S_2 = stress corresponding to 40 % ultimate load; E = chord modulus of elasticity, MPa; ε_2 = longitudinal strain produced by stress S_2.

The Eq. 1 was used to determine the static elastic modulus of the concrete specimens. The gradient of the load displacement plot was recorded as the static elastic modulus (GPa). Meanwhile the Poisson ratio was estimated from the axial and transverse strains corresponding to 40 % of the ultimate load.

2.3.4. Ultrasonic pulse velocity (UPV) dynamic elastic modulus

For determining the evolution of dynamic properties of the concrete mixes, triplicate 100 × 100 mm cubes were used for measuring the dynamic elastic modulus at curing ages of 2, 7, 28, 90 and 180 days. The non-destructive ultrasonic pulse velocity technique was implemented based on the BS EN 12504–4:2021 [52], using a Proceq Pundit PL-200PE test kit connected with 250 kHz compressional wave transducers and a receiver. Prior to every test, an OLYMPUS-supplied shear wave couplant was applied on the surfaces of the receiver and to facilitate wave propagation. This was followed by a test run for transit time using a manufacturer-supplied calibration block, where a 25.4μS value indicated very high reliability of the test. For any given cubic sample, the transducer and receiver setup (each positioned at opposite ends of the tested cube) was used to measure the wave propagation transit time. Two measurements were taken per specimen on two opposite surfaces other than the as-cast surface. Prior to testing, the mass of the three concrete cubes per mix was measured in accordance with [53]. Then, the density was calculated as the mass per unit volume (dimensional). Based on data collected, the UPV dynamic elastic, E_{dyn} (GPa) was calculated with Eq. 2 as per the ASTM C 597 [54].

$$E_{dyn} = V_p^2 \rho(1+\nu)(1-2\nu)/(1-\nu) \quad (2)$$

Where E_{dyn} = dynamic elastic modulus ρ = density (Kg/m^3), υ= Poisson ratio, V (m/s) = velocity computed from transit time

It must be highlighted that, while the Eq. 2 suggests the use of dynamic Poisson ratio for the computation of dynamic elastic modulus, the increase in strength and maturity of concrete tends to influence the Poisson ratio so that the values of static Poisson ratio and dynamic ratio appear to converge with time [55]. Thus, in this study the Poisson ratio adopted in the E_{dyn} calculation is based on the static poison ratio.

2.3.5. Bulk conductivity

Bulk conductivity provides useful information on the pore's continuity in the matrix of hardened concretes. This was performed on cylindrical samples (100Ø × 50 mm) as for the chloride permeability testing. Prior to initiating permeability test (described in Section 2.3.6), the bulk conductivity was recorded by subjecting the specimens to 60 Volts for a duration of 60 s using the potentiostat operated by the Proove'it software. The software then returns the values of bulk conductivity (mS/m) after the test duration. This automated test followed the ASTM C 1760 testing method [56]. Three cylindrical samples per concrete mix were tested per age.

2.3.6. Chloride permeability/migration testing

The Nordtest NTBUILD 492 chloride migration test [57] was adopted for studying the resistance of the concrete specimens to chloride ingress. The chloride permeability test was conducted on concretes after 28, 90 and 180 days of curing. The 100Ø × 50(±5) mm specimens cut from 100Ø × 200 mm cylinders were used for the test. About 15 mm was cut off from the as-cast surface and the bottom of the specimens and then equal thickness of (50 ± 5) mm were then obtained from the remaining section. After cutting, the circumference of the surface dried cylinders was coated with a Sika® primer (3 A:1B) and allowed to dry in a fume cupboard for 24-hours.

For all concretes whose chloride permeability was investigated, the coated specimens were preconditioned and tested as follows: the cylindrical specimens were placed in an 18 L preconditioning steel vessel. The vessel was covered and subjected to vacuum treatment pump for 3hrs. The vessel was then filled with saturated lime (~3 g/L) by opening a valve connecting a hosepipe from 5 L glass bottle to the vessel. Once all samples were fully immersed in lime solution, the valve was closed and set up allowed to continue running under vacuum for a further 1 h followed by soaking the specimen fully immersed for 18 h, and not under vacuum.

The chloride migration test was carried out in a Germann instrument PROOVE'it equipment (with associated software) by applying an electrical potential across the concrete specimens with 10 wt% NaCl solution and 0.3 M NaOH as catholyte and anolyte solution, respectively. Meanwhile a temperature sensor in the NaCl logged the temperature evolution during test time. Following a predetermined test duration (based on adjusted current recorded after applying 30 V over 60 s), the exposed surfaces were cleaned under running water. The tested cylinders were then split axially into two halves thereafter. The chloride penetration depth was measured from white precipitates formed on samples after 0.1 M $AgNO_3$ spraying of the freshly split surfaces. Seven chloride depth data points were recorded per each halved cylinder. The average chloride depths, initial and final temperature, in addition to applied voltage were used as input to calculate the non-steady-state chloride migration coefficient (D_{nssm} ×10^{-12} m^2/s) according to Eq. 3.

$$Dnssm = \frac{0.0239 * L * (T+273)}{t * (P-2)} * \left(\overline{x} - 0.0238 \sqrt{\frac{(T+273) * L * \overline{x}}{P-2}} \right) \quad (3)$$

Where; P (V) = absolute value of the potential difference applied; T (°C) = mean value of initial and final temperature in the anolyte (NaCl) solution; $\bar{X}$ (mm) = mean value of measured chloride depths; t (hour) = testing time; and L (mm) = average thickness of test piece measured across four points

2.3.7. Surface resistivity

The surface resistivity is a non-destructive rapid electrochemical technique used for concrete structural health monitoring. It was determined using a handheld Proceq resipod device that operated based on the Wenner 4-probe resistivity measurement. The four probes of the resipod equidistant to each other were axially attached to the concrete, so that current is applied via the outer probes, and inner probes measure the voltage. The device is calibrated to return the resistivity (kΩ*cm) on its display. Test was conducted on concrete cylinders immediately they were taken out of the moist room. A total of nine readings were taken per cylinder.

2.3.8. Sorptivity and porosity

The sorptivity test was conducted to assess the water admissibility of concrete. Samples for sorptivity were obtained from saw cutting the bulk cylindrical specimens. Before cutting, concrete specimens were coated with epoxy on the circumference. The test was conducted following the BS EN 13057:2002 testing method [58]. Prior to the test, samples were precondtioned by drying in a ventilated oven at (105 ± 5 °C), based on [59], as initial trials demonstrated the drying process was effective at this temperature towards achieving stabilised mass changes in 7 days, relative to studies where constant mass was achieved in 2 months drying at 50 °C [60]. While varied lower pre-conditioning temperatures [29,61] have been implemented in other studies, for reasons such as thermal gradient induced cracking or phase assemblage decomposition, trial studies on mortars or concretes showed no such indication. Also, it was decided to test the samples as per standard, so the results can be compared with those obtained in real practice, and not only used for research purposes. After oven drying, samples were cooled to room temperature in a desiccator for 24 h until testing. The samples were placed in flat-bottomed container supported with angled (L-shaped) polyvinyl chloride (PVC) pipe, such that water level traversed about 3 mm from the immersed surface of the tested sample. The mass of the cooled oven-dried sample was measured prior to the test. Then mass changes after immersion were further measured at predetermined durations up to 15 days.

Porosities of samples used for sorptivity test were further determined under vacuum saturation. This involved placement of samples in an 18 L metal vessel and under vacuum for 3 h, followed by addition of deionised water to fill to a level just above the samples. The setup was further allowed to run under vacuum for further one hour, and then vacuum turned off thereafter. Samples were kept fully immersed in water for further 24 h. Then after the surface dried mass post water saturation were measured. Porosity was computed as the ratio of mass differences to sample volume expressed a percentage. The water absorption was determined as the difference between dried and saturated mass expressed as a percentage.

3. Results and discussion

3.1. Fresh state properties

The fresh state properties of the concrete mixes are summarised in Table 3. The slump and flow classes conform to S4 (150–220 mm) and F4 (490–550 mm) respectively as per the BS EN 206:2013 +A2:2021 [44]. Fresh densities attained indicate normal weight concretes, and air content was similar for all mixes. It is noted that the addition of limestone in the slag Portland blended concretes led to a slightly improved workability compared to concretes without limestone, as reflected in the consistency and the flow diameter. These results are consistent with the fresh properties reported for similar concrete mixes prepared with the finer CEM I 52.5 R cement [29]. Overall, the fresh properties including the air content are comparable to those of CEM I concrete. For slag blended concrete it has been reported that the water to binder (w/b) and aggregate to binder (a/b) ratio are the key factors influencing slump retention, with higher ratios leading to the reduced total slump, this varying depending on the slag content in the concrete mix [62]. Given all the concretes evaluated in this study were designed with similar w/b and a/b ratios the slight changes in fresh state properties are likely linked to the different fineness of the binder's components, and the reactivity indexes of the slag used, which control the binder reaction kinetics [17,63].

Table 3
Fresh state properties of binary and ternary blended concretes.

Mix ID	Slump (mm)	Flow diameter (mm)	Air content (%)	Density (Kg/m^3)
N	185	520	1.2	2330
NS	170	480	1.1	2350
NSL	190	540	1.5	2330
NS2L	180	500	1.2	2340

3.2. Mechanical performance

3.2.1. Compressive and flexural strength

The compressive strength evolution of the concrete produced, up to 365 days of curing, is shown Fig. 4(a). Binary and ternary concrete showed significantly reduced strength (40 % reduction) at 2 days of curing compared with CEM I, albeit still meeting the typical target strengths criteria of ~10 MPa for formworks removal in construction practice [64,65]. However, continuous strength gain is observed for all concrete mixes at later ages. It is worth noting that, the replacement of slag with limestone had smaller effect on the strength values, particularly after 28 days of curing. The strength ratios ($f_{cm,2}/f_{cm,28}$) obtained for composite binders (0.3–0.4), and CEM I (0.6) show medium and rapid development respectively, according to what is suggested in [44]. All composite concretes approached strengths closer to that of CEM I concretes by 28 days of curing, and progressively increased when cured for 365 days. At 28 days of curing NS, NSL and NS2L achieved ~84, 75 and 78 % of the compressive strength exhibited by the CEM I concrete. At later curing ages (e.g. 180 days), those mixes reached 92, 84 and 80 % of the CEM I concrete strength respectively. There is no marked difference in the compressive strength values of ternary blended concrete with 10 wt% or 20 wt% limestone addition, demonstrating the limited dilution effect arising from increased limestone addition. The compressive strength evolution observed here is consistent with what has been reported for same curing ages in other studies, where 20 wt% limestone additions show lower compressive strength to CEM III/A and CEM I [28,29].

Models exist for time dependent prectiction of compressive strength, such as the ACI 209 R [66], which is an empirical model that can be described as in Eq. 4. This relationship considers the strength ratio for any curing time to the 28 days strength. Although the ACI 209 models are explicitly developed for shrinkage and creep prediction of concrete, the model also provides equations for the predictions of other mechanical performance properties such as elastic modulus and compressive strength development. The results shown in Fig. 2(b) indicate that the existing time-dependent compressive strength development models available are conservative for blended composite concretes especially with respect to later age compressive strength predictions, which is commonly seen in concrete with SCM addition. Further calibration of constants to potentially improve the accuracy of long-term compressive strength prediction are required.

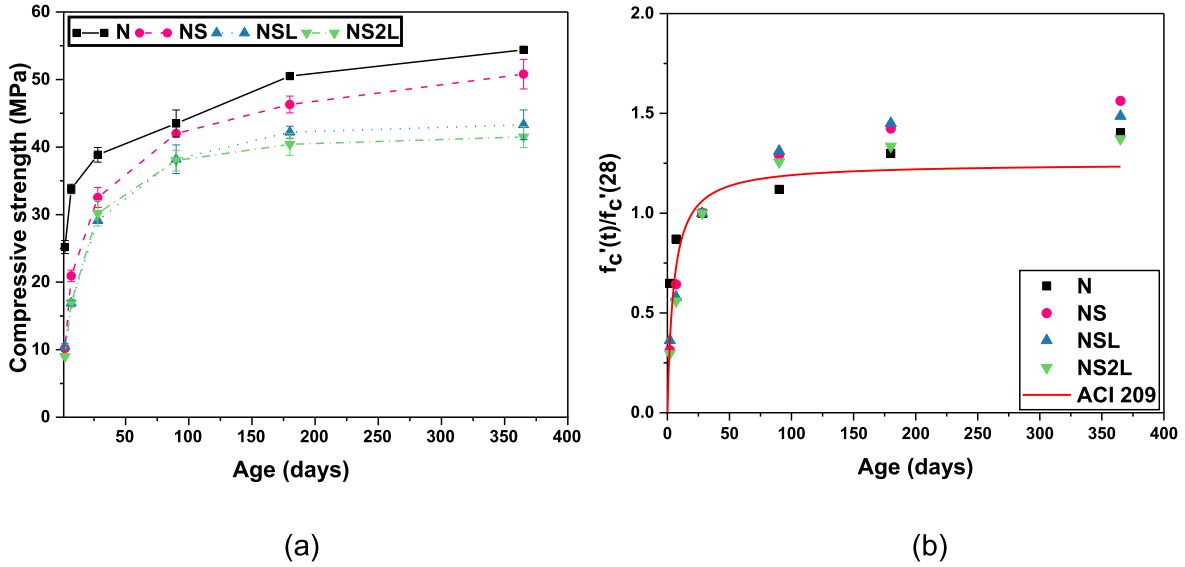

Fig. 2. (a) Compressive strength development of cured concrete mixes (error bars corresponds to one standard deviation of three measurements), (b) Comparison of strength ratios with ACI 209 R prediction models (strength are based on cube converted strength; cylinder strength (experimentally determined) = 0.8 * cube strength).

$$\frac{f_c'(t)}{f_c'(28)} = \frac{t}{\alpha + \beta t} \quad (4)$$

where; $f_c'(t)$ = compressive strength of concrete at any time t; $f_c'(28)$ = mean 28 days compressive strength (cylinder), and α, β = constants depending on cement and curing type, and appears not to be affected by aggregate (all-light weight, normal weight, and sand lightweight) type

For a 150Ø × 300 mm cylinder, the model recommends constant values of α = 4, β= 0.85 for moist room cure type 1 cement. Assuming the model is valid for the ternary and binary mixes evaluated here, the strength ratios of experimental compressive strength at all ages, in comparison to ACI 209 R strength ratios are shown in Fig. 4(b). It can be seen that CEM I shows slightly higher strength ratios at the early curing ages, while the slag containing concretes, with or without limestone, exhibited lower strength ratio than that predicted by the ACI 209 R. At 28 days and 90 days of curing, CEM I concrete conforms to the ACI-209R with a significant increase, thereafter, demonstrating that this relationship underestimates the strength gain of such concrete beyond 90 days of curing. In the case of NS, NSL and NS2L a progressively higher strength ratios than CEM I, from 28 days of curing onward, are observed. The early age compressive strength predicted by applying the equation recommended by ACI-209R agrees with the BS EN 206:2013 +A2 [44] classification of strength development based on the strength ratios ($f_{cm,2}/f_{cm,28}$), thus while the composite cements show lower early age strength development, after 28 days their rate of strength development progressively exceeds that of CEM I-based concrete.

The flexural strength of 28 and 180 days cured samples reported in Fig. 3 shows that the composite concrete exhibit comparable strength to CEM I-based concrete at early (28 days) and at extended curing ages. The contribution of slag replacement in improving flexural strength of concrete is consistent with the findings of Khatib and Hibbert [67]. It does appear that the replacement of slag content with up to 20 wt% limestone has no adverse impact on the flexural strength of ternary blends, as the values increase at later ages relative to those obtained in binary slag blended concrete. The comparable performance under bending loads of the concrete assessed, despite the different compressive strengths recorded, can be attributed to the refined microstructure due to secondary hydration or better packing density in slag blended concrete relative to CEM I, particularly around the more porous interfacial transition zone (ITZ) [68,69]. Thus, an improvement in the bond strength of ITZ in NS, NSL and NS2L is likely to contributing to their flexure strength performance, particularly for NSL and NS2L at later curing ages. However, this needs to be evaluated.

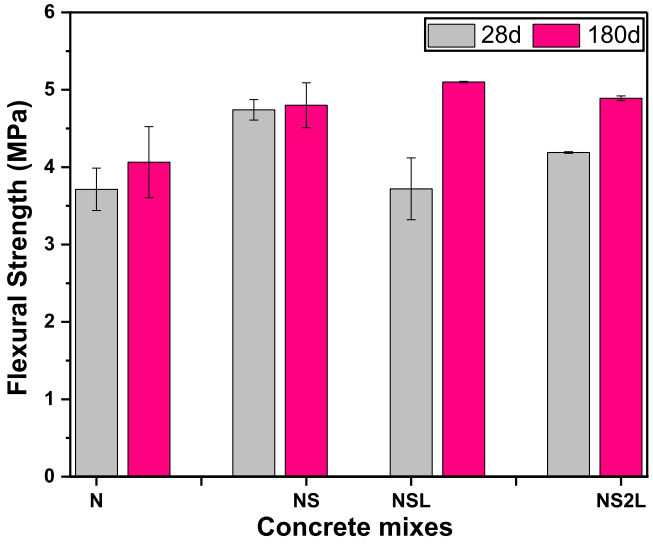

Fig. 3. Flexural strength evolution of binary and ternary slag Portland blended concrete prisms, as a function of the curing duration and limestone content. Error bars corresponds to one standard deviation of two measurements.

3.2.1.1. Empirical and experimental relationship between compressive strength and flexural strength. Design codes, standards and researchers have proposed different approaches to estimate flexural strength from the compressive strength values of concrete using analytical relationships. For emerging concretes produced with ternary blended cements, it is important to ascertain the extent of over/under estimation when using these equations to determine their applicability. Fig. 4 shows experimentally determined flexural strengths in comparison with estimated values based on empirical equations (shown in Table 4) using experimentally determined 28 and 180 days compressive cylindrical strengths as input.

Where F_r is the flexural strength f'c is the compressive strength and λ

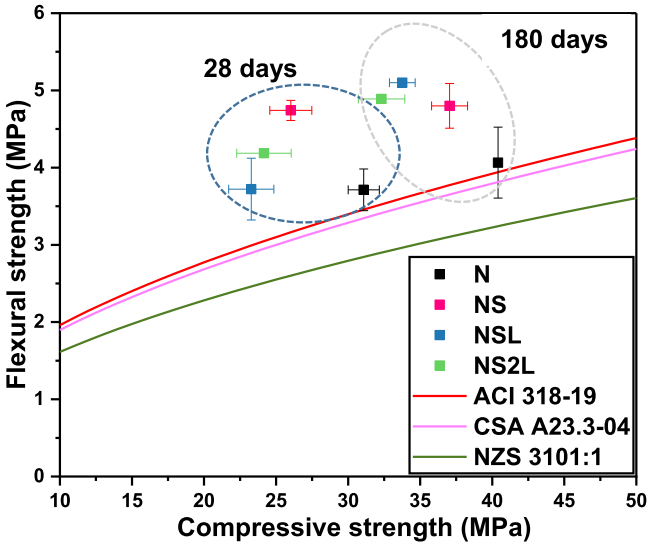

Fig. 4. Applicability of existing codes' relationships between flexural and compressive strengths to the binary and ternary slag blended concrete studied.

Table 4
Empirical equation for flexural strength prediction from compressive strength.

Design code	Equation (MPa)	Reference
ACI 318 – 19	$Fr = 0.62 * \lambda * (f'_c)^{0.5}$; $\lambda = 1.00$	[70]
CSA A23.3–04	$Fr = 0.6\ \lambda\ (f'_c)^{0.5}$; $\lambda = 1.00$	[71]
NZS 3101:1–2006	$Fr = 0.6\ \lambda\ (f'_c)^{0.5}$; $\lambda = 0.85$	[72]

is constant based on composition of aggregates or equilibrium density of concrete [normal weight concrete in this case]

The results in Fig. 4 show that all the concrete mixes assessed exceed the values predicted by the three codes evaluated, indicating that any of these codes can safely be adopted for predicting the values of flexural strength achieved by binary and ternary slag concretes. This suggests that concrete made from slag composite cements with limestone addition can perform satisfactorily as structural concrete, according to existing strength prediction equations proposed by design codes.

3.2.1.2. Poisson ratio determination. The Poisson ratio determined experimentally was used as input to calculate the dynamic elastic modulus for the evaluated concretes. It was determined from the axial and transverse strains corresponding to 40 % of the ultimate load. The computed values for N, NS, NSL and NS2L were 0.13 ± 0.02, 0.14 ± 0.003, 0.15 ± 0.03, and 0.15 ± 0.012, respectively. Concrete with binary and ternary cements had slightly higher Poisson ratio than CEM I-based concrete. The obtained results approach typical values recommended by design codes, such as BS EN 1992–1–1:2023 (Eurocode 2) and *fib* model code, where a general Poisson ratio of 0.2 and 0 are prescribed, for uncracked and cracked concrete respectively [73,74]. However, as experimentally determined Poisson ratio for concretes made with ternary composite binders containing limestone are not often reported in the open literature, the likelihood for overdesign arising from the use of conservative values recommended by design codes is inevitable. Such tendencies are interrogated by comparative analysis on dynamic modulus elasticity computed using experimentally determined Poisson ratio and values specified by BS EN 1992–1–1:2023 (Eurocode 2) in subsequent sections.

3.2.1.3. Static and dynamic modulus of elasticity. The modulus of elasticity of concrete is an important structural design parameter. It is pertinent for serviceability compliance in structural design e.g. for controlling deflection and estimating creep limit states and allowable sway of structures [70]. It indicates the stiffness of concrete, and it is typically related to the density of concrete and compressive strength of concrete using analytical relationship that are commonly used to estimate elastic-modulus for structural design [73,75,76]. Fig. 5(a) shows the static modulus of elasticity of the concrete mixes evaluated. The cylinder compressive strength of N, NS, NSL, and NS2L at the time of testing were 29.8, 29.2, 25.4, and 26.2 MPa, respectively, corresponding to cylinder/cube strength of approximately 0.8 for all the mixes. It is identified that slag containing concretes with/without limestone exhibited comparable elastic behaviour to CEM I under static loads, as reflected in the stress strain relationship as shown in Fig. 5(b).

Additionally, the dynamic elastic modulus of concrete mixes was calculated using Eq. 2. In Fig. 6(a), the evolution of the dynamic modulus for the concrete mixes evaluated is reported. The dynamic elastic modulus of all concrete mixes increased with curing age. Composite cement concrete shows relatively lower modulus from 2 days compared with CEM I concrete, but a significant increase is observed from 7 days of curing onward, and compares with CEM I concrete by 28 days of curing and at advanced curing ages. The results are consistent with other studies particularly at the early ages [77]. The UPV dynamic elastic modulus evolves similarly to the compressive strength as shown in Fig. 6(b). Overall, the elastic properties of concrete can be influenced by the aggregate's fraction. Factors such as the aggregate and cement paste interface would play significant role, as failure would typically proceed in those regions under load for matured concretes. The plausible refinement of microstructure of concrete, particularly in the ITZ regions typically reported for slag cement concrete [78] likely improves the static and dynamic moduli relative to CEM I-concrete for the tested curing ages.

A comparison between experimentally determined dynamic elastic modulus and the estimated values calculated according to the BS EN 1992–1–1:2023 (Eurocode 2) or the *fib* model code, which recommends a Poisson ratio of 0.2 for uncracked concrete, was conducted, and the results are shown in Fig. 7(a). It can be seen that a direct correlation exists between the experimental data and estimated results based on Poisson ratios recommended by the design codes. This indicates that the proposed values in design codes can be satisfactorily used for the structural design of concrete made with the composite cement assessed in this study.

Despite the potential applicability of the Poisson ratio for the structural design of composite cement, a comparison (see Fig. 7(b)) of dynamic modulus calculated using the experimentally determined Poisson ratios or the prescribed value of 0.2 in the codes was conducted. It was identified that the computed dynamic modulus based on experimental Poisson values yields nearly + 5 GPa more than computation based on recommended values such Poisson ratio prescribed in the BS EN 1992–1–1:2023 (Eurocode 2) or *fib* code. Considering reinforcement bar requirement in structural design is typically dependent on the elastic modulus and Poisson ratios [51], the results here suggest that potential savings in quantities required of concrete cover layer can be achieved by minimising overdesign while using binary or ternary slag blended concretes.

3.2.1.4. Correlation of compressive strength and static elastic modulus. Table 5 shows a summary of analytical equations used for estimating static elastic modulus from the mean 28 days compressive strength. Fig. 8 shows a plot comparing experimentally determined values versus estimates from empirical equations.

The results indicate that slag blended concretes with up to 20 wt% limestone addition evaluated in this study can perform satisfactorily as per existing strength-modulus relationships in structural concrete standards. The *fib* model code and Eurocode 2 appears to exhibit better predictability for concrete mixes assessed here, than the more conservative ACI-318, NZS 3101:1 and CSA A23.3–04.

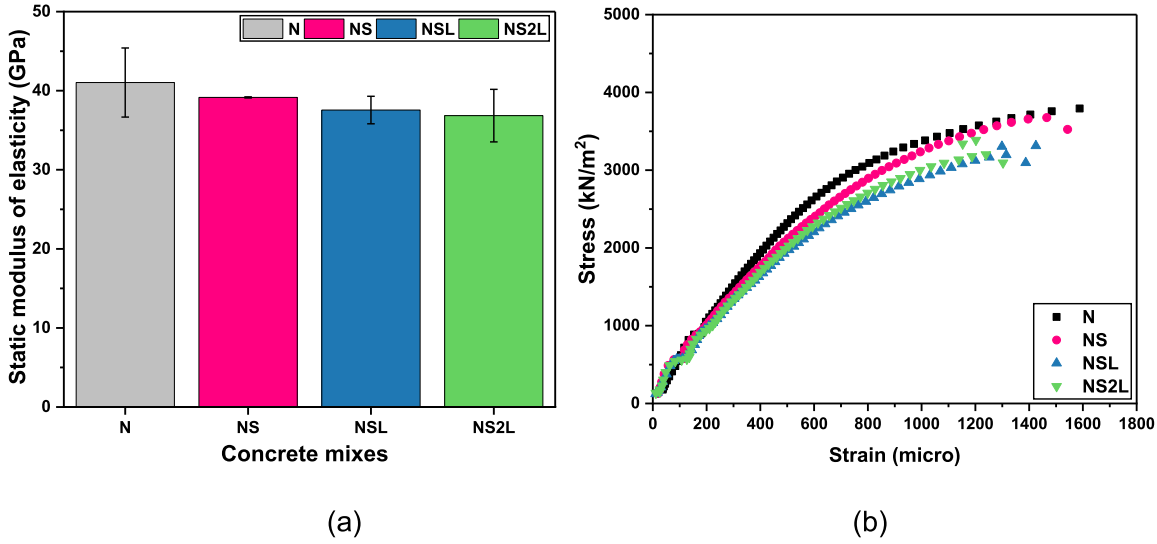

Fig. 5. (a) Static elastic modulus of concrete mixes (28 days cured). Error bars correspond to one standard deviation of two measurements; and (b) stress-strain relationship of concrete mixes (28 days cured).

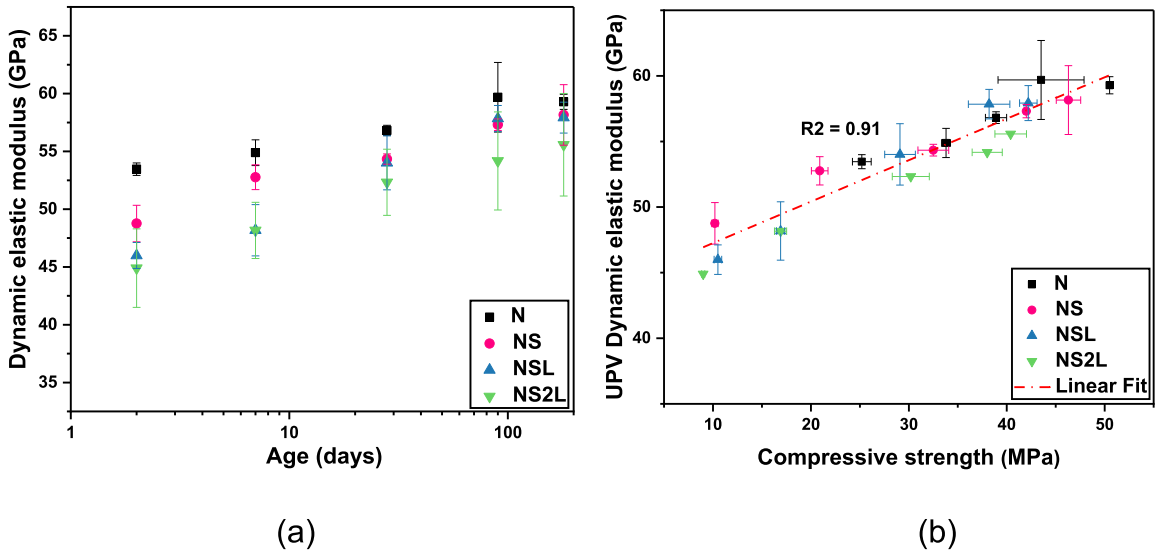

Fig. 6. (a) Dynamic modulus of elasticity evolution of cured concrete mixes (error bars correspond to one standard deviation of three measurements) calculated using experimentally determined Poisson ratios; and (b) linear regression between compressive strength and dynamic elastic modulus of concrete mixes.

3.2.2. *Durability performance*

3.2.2.1. Sorptivity and total porosity. The sorptivity of concrete gives a measure of one-dimensional water admissibility in the capillary pores with respect to time, driven by interfacial pressure gradients, and is generally used as an indirect durability indicator of pore structure variations in cementitious materials. Sorptivity profiles are obtained plotting the mass changes as a function of the square root of time.

Fig. 9 shows the sorptivity profile of concrete mixes cured for 28, 90 and 180 days. No significant difference in water absorption rates was observed for the concrete NS, NSL and NS2L at 28 and 180 days of curing. The kinetics of water ingress can be quantified by the sorptivity coefficient. The sorptivity coefficients (slope of the initial linear portion of sorptivity profile) of the concrete mixes evaluated are reported in Table 6, where it can be seen that composite binders show comparable sorptivity coefficients by 180 days compared to CEM I-based concrete. The results show that the replacement of slag by 20 wt% limestone has no significant impact on the water absorption properties of the concrete mixes evaluated, consistent with the similarities in the total water absorbed at all ages. The improved water absorption properties can be attributed to the progressive densification of microstructure with curing age, this likely linked to the pore refinement in the composite cements contributing to their resistance to moisture ingress. The results are consistent with other studies that report a reduction in water admissibility in concrete with limestone addition [29,79].

Furthermore, the results of the total porosity of concrete mixes are shown in Fig. 10. It is observed that the porosity is comparable for all mixes with curing time, with an overall reduction in porosities at prolonged curing durations (when considered within error margins). Considering the classification of concrete durability potential based on the porosities for SCM-containing concrete mixes proposed by Baroghel-Bouny et al. [80], it is identified that all the concretes assessed can be classified to present high to medium durability.

3.2.2.2. Bulk conductivity. Fig. 11 shows bulk conductivities of the concretes studied as a function of their curing age. Higher conductivities

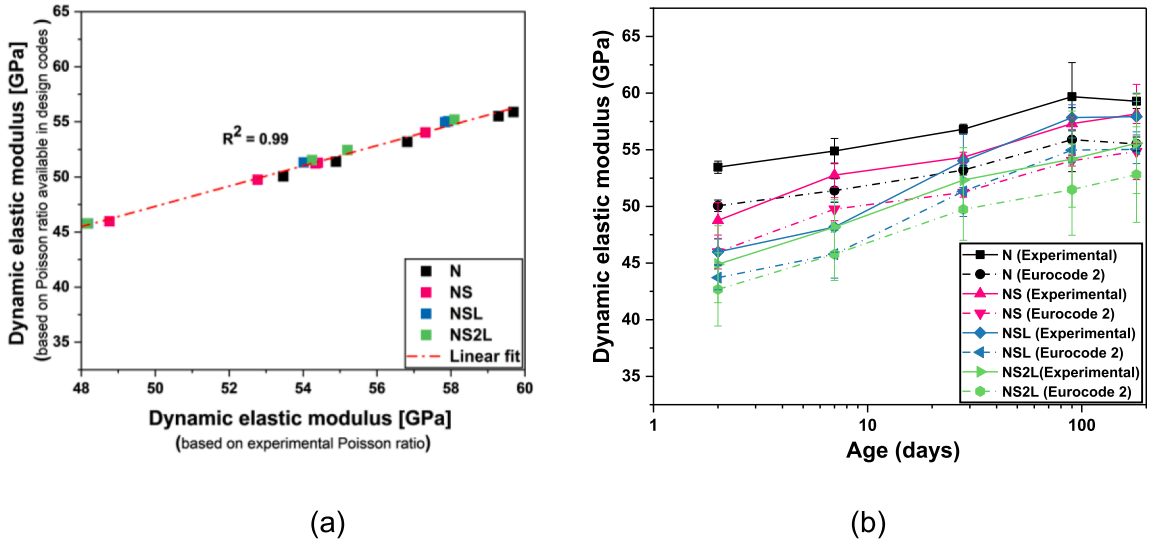

Fig. 7. (a) Correlation between dynamic modulus of elasticity based on experimental Poisson ratio and a Poisson ratio of 0.2 as per design codes (*fib*/Eurocode 2) for uncracked concrete; and (b) Evolution of dynamic modulus of elasticity calculated using the experimentally determined Poisson ratio or the Poisson ratio (0.2) recommended in *fib*/Eurocode 2 design codes.

Table 5
Empirical equations for static modulus prediction from compressive strength.

Design code	Equation (GPa)	Reference
ACI 318–19	$4700*(f_c^{0.5})$	[70]
fib	$(21.5*10^3)*(f_c/10)^{1/3}$	[73]
BS EN 1992–1–1:2023 (Eurocode 2)	$9500*f_{cm}^{1/3}$	[74]
CSA A23.3–04	$4500*(f`_c)^{0.5}$	[71]
NZS3101:1–2006	$3220(f`_c)^{0.5}+6900$	[72]

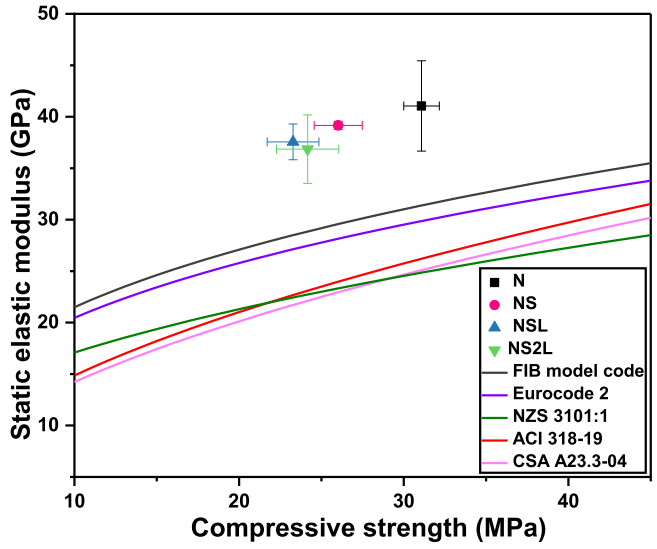

Fig. 8. Static elastic modulus of binary and ternary slag blended of 28 day cured concrete. Experimentally determined versus existing empirical models.

(lower resistivities) are recorded in CEM I concrete relative to composite binders, at all curing ages evaluated. Among the blended concretes evaluated, the conductivity value reduced at an increased in curing duration from 28 to 180 days. The difference in the conductivity values between NS, NSL and NS2L is quite modest compared to CEM I-based concrete, demonstrating that concrete produced with composite cements with up to 20 wt% limestone has a comparable bulk conductivity to that of binary slag concrete. Based on these results it could be inferred that the resistance to corrosion of steel reinforcement of concretes produced with slag, or slag + limestone cements is likely to be higher than that of CEM I concrete, however this does not account for the ionic composition of the pore solution and sulfide species in slags whose oxidation might influence the bulk conductivity measurement [81,82]. Therefore, there is a need to exercise caution in the use of bulk conductivity to comprehensively infer corrosion resistance of steel reinforcement in the composite concretes. It is well accepted that the conductivity of concrete bulk also influence the corrosion rate of steel reinforcement in blended concretes along with other factors such as moisture state, the microstructure of the at the steel-concrete-interface, pore solution composition and the cover depth [83,84]. Recent studies have also related bulk conductivity to long term chloride penetration depth in different binder types [85] which highlights the potential durability implications from lower bulk conductivity of slag and slag-limestone composite concretes.

The reduced conductivities potentially arises from discontinuities in the pores structure or increased tortuosity in the composite binders relative to CEM I [36,86] leading to differences in the internal degree of saturation of the concretes, and also the differences in the ionic composition of the pore water with changes in the binder chemistry.

3.2.2.3. Surface resistivity of concrete. The surface resistivity test is a rapid non-destructive test used for structural health monitoring of concrete structures as an indicator for susceptibility to corrosion, so that higher surface resistivity would suggest reduced risk of corrosion and vice versa. In Fig. 12(a), surface resistivities of the concrete mixes are reported. It is identified that the surface resistivity increased with the replacement of CEM I by slag or slag + limestone, being higher in mixes with 10 wt% limestone. This difference is significantly more notable at extended curing ages (90 days) where the surface resistivity values of binary or ternary cement-based concretes is 2–3 folds higher than those of CEM I concrete. These results can be attributed to more refined pore structure in slag concretes with or with/without limestone with curing time [11]. While this result appears to suggest a potentially reduced risk to corrosion, it must be recognised that the pore solution of the composite systems has reduced alkalis compared to CEM I [82,87], so the response to the resistivity test requires further evaluation to determine the true impact of higher resistivities obtained in composite cement concrete on corrosion potential in reinforced concrete.

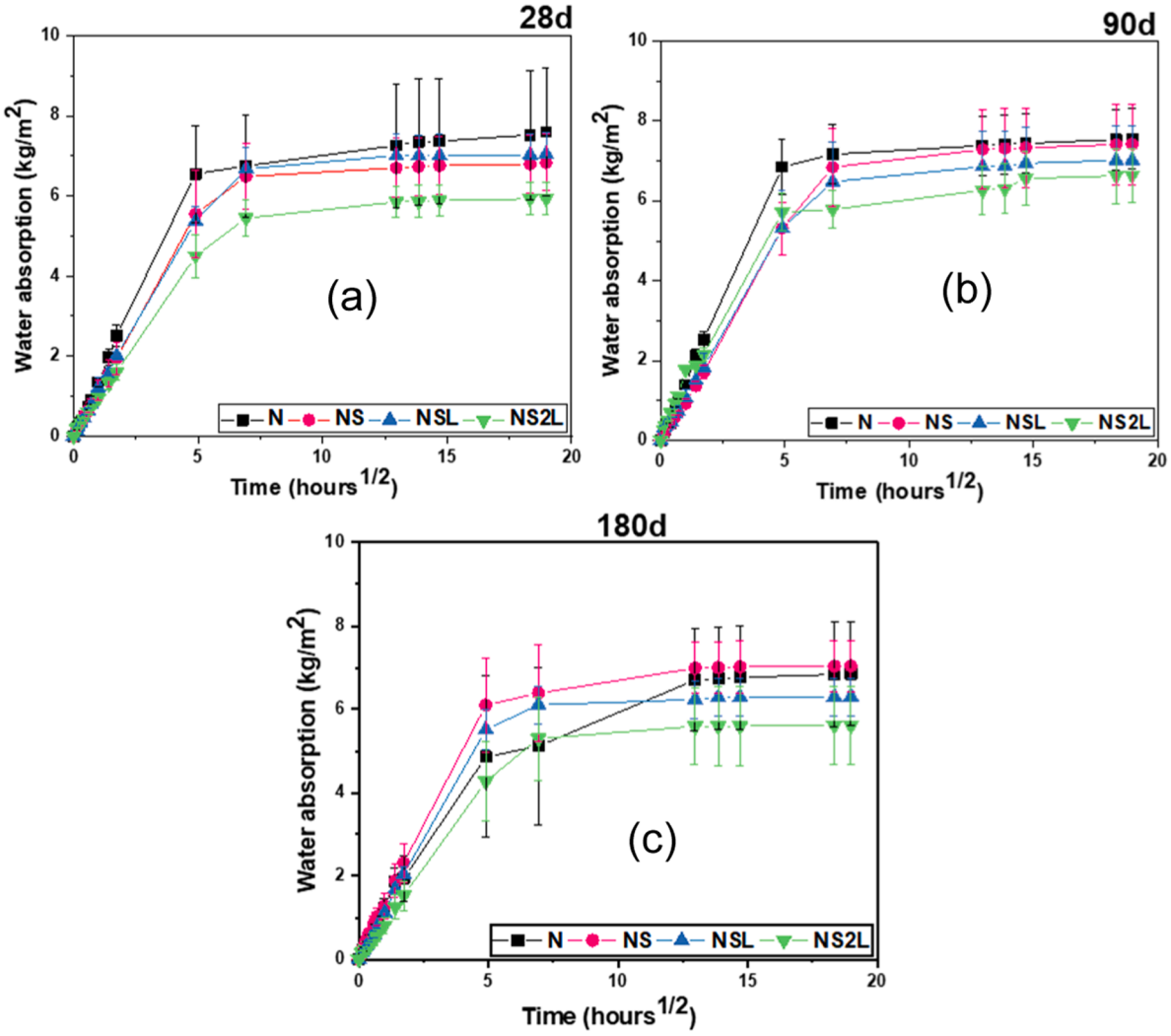

Fig. 9. Sorptivity profiles of binary and ternary concretes after curing for (a) 28 days (b) 90 days and (c) 180 days. Average curves of two tested samples are reported, with error bars corresponding to one standard deviation of two curves.

Table 6
Sorptivity coefficients ($kg*m^{-2}*h^{-0.5}$) of moist cured concrete mixes.

Cured Age	Mix ID			
	N	NS	NSL	NS2L
28	1.08 ± 0.26	0.99 ± 0.18	0.99 ± 0.08	0.81 ± 0.10
90	1.13 ± 0.15	1.01 ± 0.17	0.96 ± 0.18	0.89 ± 0.10
180	0.96 ± 0.19	0.99 ± 0.22	0.94 ± 0.09	0.79 ± 0.19

Table 7
Total water absorption (%mass) of moist room cured concretes.

Cured Age	Mix ID			
	N	NS	NSL	NS2L
28	6.02 ± 1.53	5.43 ± 1.06	5.93 ± 0.44	5.09 ± 0.63
90	5.70 ± 1.19	6.09 ± 1.21	5.92 ± 0.39	5.11 ± 1.28
180	5.34 ± 1.2	6.28 ± 1.46	5.62 ± 0.52	4.90 ± 0.70

Meanwhile, the correlation between bulk conductivity and surface resistivity of the concrete studied (Fig. 12) is consistent with results reported in other studies [88,89], however the meaning and relevance of this relationship for concretes with SCMs needs to be further investigated.

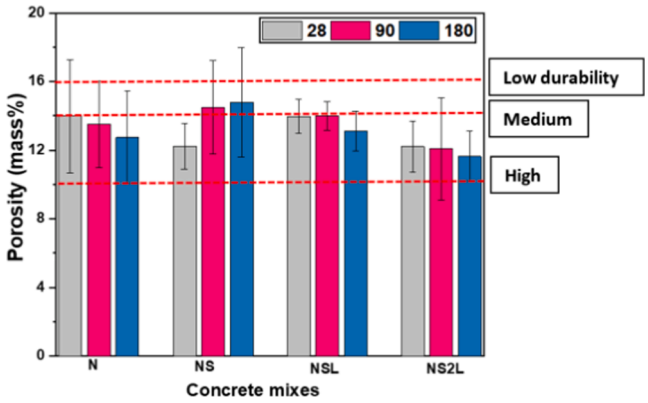

Fig. 10. Porosity of concrete mixes (error bars corresponds one standard deviation of three measurements); classification based on Baroghel-Bouny et al. [80].

3.2.2.4. Resistance to chloride ions ingress. The NordTest NTBuild 492 has been identified as a relatively precise non steady state method of investigating chloride ingress in SCM containing concretes, when compared to other migration/diffusion test methods [90]. The results of chloride migration are shown in Fig. 13. The calculated non-steady state

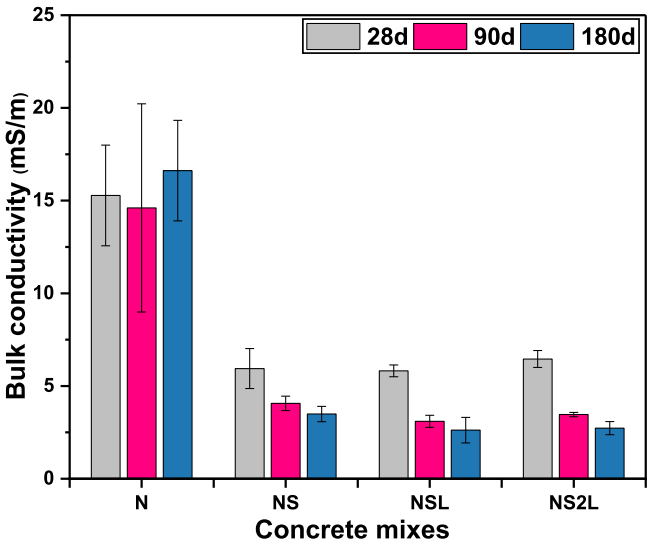

Fig. 11. Bulk conductivity on concrete mixes (error bars corresponds to one standard deviation of three measurements).

migration coefficient shows a reduction in chloride permeability of the composite binders containing slag compared to CEM I concrete, which is consistent with what has been reported by Proske et al. [28]. The chloride coefficient decreases with curing age for all concrete mixes. While NS shows the lowest migration coefficient after 28 days curing, the reduction with curing time is not significant, in comparison to the ternary blends, where up to ~50 % reduction is observed in their migration coefficients and approaches values of NS at advanced ages.

In a slag rich concrete, chloride resistances may be attributed to the formation of Friedel's salt arising from binding between slag hydration products and chloride ions [91], including the likelihood of chlorides binding to hydrotalcite like phases [26]; however, the NTBuild 492 is limited in accounting for such contributions. The assumption of a constant chlorides binding capacity and the possibility its reduction with test duration when applying a voltage as suggested in [90] is expected to impact the overall binding of chlorides taken place in the material. However, this is an artifact of the test rather than a true representation that chloride binding is somehow reduced for a given cementitious system. Fig. 14 shows a linear correlation between the bulk conductivity and the chloride migration coefficient for the concrete mixes assessed, so that higher bulk conductivities are observed in concrete with the higher chloride migration coefficients. The trend is similar to previous studies on other SCMs blended cements [87,92]. Based on durability classifications proposed by Baroghel-Bouny et al. [80,93]; NS, NSL and NSL demonstrate medium to high resistance to chloride permeability which improves with curing age, while N exhibits low chloride permeability. The results suggest that reducing slag content by 20 wt% with limestone addition has a negligible effect on the chloride permeability of the concrete evaluated, and such concrete reports excellent performance compared to CEM I.

4. Conclusions

Based on the experimental findings on mechanical performance and durability properties of concrete with CEM I, binary cement with 50 wt % blast furnace slag, ternary cements with slag plus 10 wt% limestone and slag plus 20 wt% limestone, the following conclusions are reached:

1. After 2-days of curing the compressive strengths of concrete produced with binary or ternary cements are about 40 % lower than that of concrete made with CEM I-based concrete. However, all concretes reached ~10 MPa or more after 2 days in compliance with requirements for formwork removal in real practice. Binary and

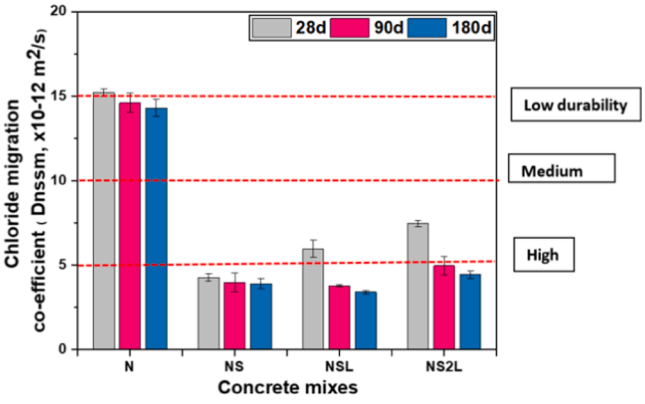

Fig. 13. Chloride migration coefficients (m^2/s) of binary and ternary slag blended concrete mixes after 28, 90 and 180 days (error bars corresponds one standard deviation of three measurements). Durability classification based on Baroghel-Bouny et al. [80].

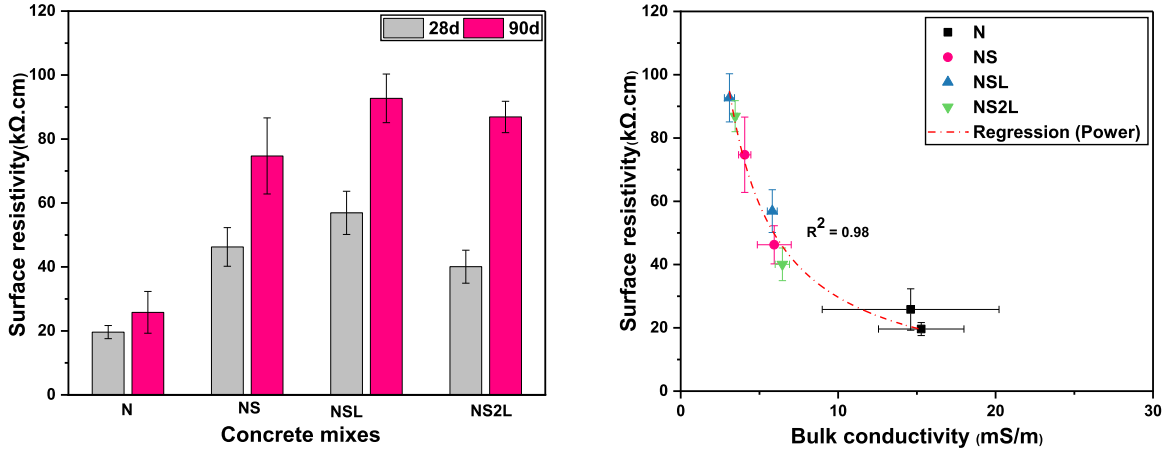

Fig. 12. Surface resistivity on binary or ternary slag blended concrete mixes (error bars corresponds to 2 cylinders); and (b) relationship between surface resistivity and bulk conductivity.

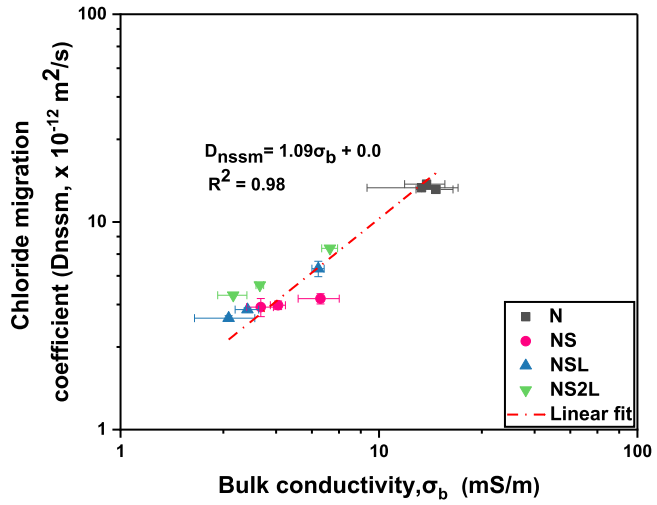

Fig. 14. Relationship between bulk conductivity and bulk chloride migration co-efficient of binary and ternary slag blended concretes at different curing ages.

ternary concretes developed a 28-day compressive strength ~30 % lower than CEM I-based concrete, but reached the design compressive strength. The compressive strength of concrete containing limestone developed rapidly after 7 days of curing, achieving strength comparable to those identified in slag-containing concretes without limestone addition.

2. Slag-containing concrete exhibit better flexural strength compared with CEM I-based concrete. The addition of 10 or 20 wt% limestone has no significant effect on the flexural strength of composite concrete, as values are comparable to those of binary slag blended concrete. Existing equations for predicting flexural strength based on compressive strength values, proposed in different structural design codes can be utilised for slag-limestone composite cements concretes.
3. The dynamic elastic modulus of slag-containing concrete, with and without limestone addition, are lower at 2-days of curing compared to CEM I-based concrete, but increase significantly after 7 days of curing, and are comparable to CEM I by 28 days and at 180 days. This suggest that for the concrete mixes evaluated in this study 28 days compressive strength values can be used for structural design purposes, conversely to what has been suggested for other concretes with SCMs, where it has been suggested that results after 56 or 90 days of curing should be used to compensate the delayed microstructure and strength development.
4. Replacing Portland cement with blast furnace slag leads to a significant reduction of the chlorides migration coefficient, and the addition of up to 20 wt% limestone slightly increased the chloride permeability of concrete, relative the binary concrete, albeit about 3 folds less than the migration coefficient of CEM I-based concrete by 180 days curing age. Correlating the bulk conductivity to chloride migration coefficients demonstrates the strong influence of pore refinement, even when the influence of chloride binding capacity due to slags is not considered.
5. The sorptivity and water accessible porosity demonstrate that slag-containing concretes with or without limestone does not exhibit detrimental water absorption properties relative to CEM I-based concrete, which is more evident at prolonged curing ages.
6. The relatively higher surface resistivity of ternary blends indicates pore refinement and increased tortuosity and the potential to reduce migration of free chlorides.

Overall, it can be concluded that replacing slag with up to 20 wt% limestone powder does not adversely affect the mechanical or durability performance of concrete. These concrete mixes exhibit satisfactory performance comparable to, not only to binary slag blended concrete (with 50 wt% slag), but to CEM I in most cases. Assessment of their conformance to design codes suggest they can be satisfactorily used as structural concrete, with the opportunity of design optimisation, as the mechanical performance exhibited by the tested concrete is superior to that predicted by the code's proposed relationships.

CRediT authorship contribution statement

Moro Sabtiwu: Writing – review & editing, Writing – original draft, Methodology, Investigation, Formal analysis, Data curation, Conceptualization. **Yuvaraj Dhandapani:** Writing – review & editing, Supervision, Methodology. **Drewniok Michal:** Writing – review & editing, Supervision. **Samuel Adu-Amankwah:** Writing – review & editing, Supervision, Methodology, Conceptualization. **Susan A. Bernal:** Writing – review & editing, Writing – original draft, Resources, Project administration, Methodology, Funding acquisition, Conceptualization.

Declaration of Competing Interest

The authors declare that they have no known competing financial interests or personal relationships that could have appeared to influence the work reported in this paper.

Acknowledgements

The PhD research of M. Sabtiwu was sponsored by the Engineering and Physical Sciences Research Council (EPSRC) via a CASE PhD studentship co-sponsored by National Highways. Participation of S.A. Bernal in this study was sponsored by the EPSRC early career fellowship EP/R001642/1.

Data Availability

The dataset derived from this study is accessible via the University of Leeds Research Data Repository in the link - https://doi.org/10.5518/1637

References

[1] I.H. Shah, S.A. Miller, D. Jiang, R.J. Myers, Cement substitution with secondary materials can reduce annual global CO_2 emissions by up to 1.3 gigatons, Nat. Commun. 13 (1) (2022) 5758.
[2] U. Environment, K.L. Scrivener, V.M. John, E.M. Gartner, Eco-efficient cements: potential economically viable solutions for a low-CO_2 cement-based materials industry, Cem. Concr. Res. 114 (2018) 2–26.
[3] Y. Dhandapani, M. Santhanam, G. Kaladharan, S. Ramanathan, Towards ternary binders involving limestone additions — a review, Cem. Concr. Res. 143 (2021) 106396.
[4] ASTM C595/C595M, Standard Specification for Blended Hydraulic Cements, ASTM International, West Conshohocken, PA, 2024.
[5] BS EN 197-1, Cement, Composition, Specifications and Conformity Criteria for Common Cements, British Standard Institution, London, England, 2011.
[6] V. Bonavetti, H. Donza, G. Menendez, O. Cabrera, E.F. Irassar, Limestone filler cement in low w/c concrete: a rational use of energy, Cem. Concr. Res. 33 (6) (2003) 865–871.
[7] N. Voglis, G. Kakali, E. Chaniotakis, S. Tsivilis, Portland-limestone cements. Their properties and hydration compared to those of other composite cements, Cem. Concr. Compos. 27 (2) (2005) 191–196.
[8] BS EN 197-5. Portland-composite cement CEM II/C-M and Composite cement CEM VI, BSI London, 2021.
[9] BS 8500-2. Concrete. Complementary British Standard to BS EN 206. Specification for constituent materials and concrete, BSI London, 2023.
[10] S. Adu-Amankwah, M. Zajac, C. Stabler, B. Lothenbach, L. Black, Influence of limestone on the hydration of ternary slag cements, Cem. Concr. Res. 100 (2017) 96–109.
[11] M. Zajac, J. Skocek, S. Adu-Amankwah, L. Black, M. Ben Haha, Impact of microstructure on the performance of composite cements: why higher total porosity can result in higher strength, Cem. Concr. Compos. 90 (2018) 178–192.
[12] M. Heikal, H. El-Didamony, M.S. Morsy, Limestone-filled pozzolanic cement, Cem. Concr. Res. 30 (11) (2000) 1827–1834.

[13] G. Ye, X. Liu, G. De Schutter, A.M. Poppe, L. Taerwe, Influence of limestone powder used as filler in SCC on hydration and microstructure of cement pastes, Cem. Concr. Compos. 29 (2) (2007) 94–102.
[14] B. Lothenbach, G. Le Saout, E. Gallucci, K. Scrivener, Influence of limestone on the hydration of Portland cements, Cem. Concr. Res. 38 (6) (2008) 848–860.
[15] V.L. Bonavetti, V.F. Rahhal, E.F. Irassar, Studies on the carboaluminate formation in limestone filler-blended cements, Cem. Concr. Res. 31 (6) (2001) 853–859.
[16] P. Mounanga, M.I.A. Khokhar, R. El Hachem, A. Loukili, Improvement of the early-age reactivity of fly ash and blast furnace slag cementitious systems using limestone filler, Mater. Struct. 44 (2) (2011) 437–453.
[17] S. Adu-Amankwah, S.A. Bernal, L. Black, Influence of component fineness on hydration and strength development in ternary slag-limestone cements, RILEM Tech. Lett. 4 (2019) 81–88.
[18] S. Krishnan, S. Bishnoi, Understanding the hydration of dolomite in cementitious systems with reactive aluminosilicates such as calcined clay, Cem. Concr. Res. 108 (2018) 116–128.
[19] K. De Weerdt, M.B. Haha, G. Le Saout, K.O. Kjellsen, H. Justnes, B. Lothenbach, Hydration mechanisms of ternary Portland cements containing limestone powder and fly ash, Cem. Concr. Res. 41 (3) (2011) 279–291.
[20] T. Matschei, B. Lothenbach, F.P. Glasser, The role of calcium carbonate in cement hydration, Cem. Concr. Res. 37 (4) (2007) 551–558.
[21] D.P. Bentz, A. Ardani, T. Barrett, S.Z. Jones, D. Lootens, M.A. Peltz, T. Sato, P. E. Stutzman, J. Tanesi, W.J. Weiss, Multi-scale investigation of the performance of limestone in concrete, Constr. Build. Mater. 75 (2015) 1–10.
[22] S. Tsivilis, G. Batis, E. Chaniotakis, G. Grigoriadis, D.J.C. Theodossis, c. research, Properties and behavior of limestone cement concrete and mortar 30 (10) (2000) 1679–1683.
[23] S. Palm, T. Proske, M. Rezvani, S. Hainer, C. Müller, C.-A. Graubner, Cements with a high limestone content – Mechanical properties, durability and ecological characteristics of the concrete, Constr. Build. Mater. 119 (2016) 308–318.
[24] P. Tennis, M. Thomas, W. Weiss, State-of-the-Art Report on Use of Limestone in Cements at Levels of up to 15%, Portland Cement Association, Skokie, Illinois, USA, 2011.
[25] A. Bahulayan, M. Santhanam, Hydration, phase assemblage and microstructure ofcementitious blends with low-grade limestone, Constr. Build. Mater. 438 (2024) 137044.
[26] A. Machner, M. Zajac, M. Ben Haha, K.O. Kjellsen, M.R. Geiker, K. De Weerdt, Chloride-binding capacity of hydrotalcite in cement pastes containing dolomite and metakaolin, Cem. Concr. Res. 107 (2018) 163–181.
[27] A. Machner, M. Zajac, M. Ben Haha, K.O. Kjellsen, M.R. Geiker, K. De Weerdt, Limitations of the hydrotalcite formation in Portland composite cement pastes containing dolomite and metakaolin, Cem. Concr. Res. 105 (2018) 1–17.
[28] T. Proske, M. Rezvani, S. Palm, C. Müller, C.-A. Graubner, Concretes made of efficient multi-composite cements with slag and limestone, Cem. Concr. Compos. 89 (2018) 107–119.
[29] S. Adu-Amankwah, M. Zajac, J. Skocek, M. Ben Haha, L. Black, Relationship between cement composition and the freeze–thaw resistance of concretes, Adv. Cem. Res. 30 (8) (2018) 387–397.
[30] P. Hawkins, P.D. Tennis, R.J. Detwiler, The use of limestone in Portland cement: a state-of-the-art review, Portland Cement Association, Skokie, IL, USA, 1996.
[31] P.D. Tennis, M.D.A. Thomas, W.J. Weiss, StateArt. Rep. Use Limest. Cem. Lev. 15% (2011).
[32] K.-S. Lauch, V. Dieryck, Durability of concrete made with ternary cements containing slag or fly ash and limestone filler, Int RILEM Conf. Mater. Syst. Struct. Civ. Eng (MSSCE), Lyngby, Denmark. PRO113 - Proceedings of the Conf. Segm. Concr. SCMs. (2016) p. 299. RILEM Publications S.A.R.L.
[33] Z. Liu, P. Van den Heede, C. Zhang, X. Shi, L. Wang, J. Li, Y. Yao, B. Lothenbach, N. De Belie, Carbonation of blast furnace slag concrete at different CO_2 concentrations: Carbonation rate, phase assemblage, microstructure and thermodynamic modelling, Cem. Concr. Res. 169 (2023) 107161.
[34] H. Vanoutrive, P. Van den Heede, N. Alderete, C. Andrade, T. Bansal, A. Camões, Ö. Cizer, N. De Belie, V. Ducman, M. Etxeberria, L. Frederickx, C. Grengg, I. Ignjatović, T.-C. Ling, Z. Liu, I. Garcia-Lodeiro, B. Lothenbach, C. Medina Martinez, J. Sanchez-Montero, K. Olonade, A. Palomo, Q.T. Phung, N. Rebolledo, M. Sakoparnig, K. Sideris, C. Thiel, T. Visalakshi, A. Vollpracht, S. von Greve-Dierfeld, J. Wei, B. Wu, M. Zając, Z. Zhao, E. Gruyaert, Report of RILEM TC 281-CCC: outcomes of a round robin on the resistance to accelerated carbonation of Portland, Portland-fly ash and blast-furnace blended cements, Mater. Struct. 55 (3) (2022) 99.
[35] M. Otieno, H. Beushausen, M. Alexander, Effect of chemical composition of slag on chloride penetration resistance of concrete, Cem. Concr. Compos. 46 (2014) 56–64.
[36] E. Berodier, K. Scrivener, Evolution of pore structure in blended systems, Cem. Concr. Res. 73 (2015) 25–35.
[37] M. Maes, E. Gruyaert, N. De Belie, Resistance of concrete with blast-furnace slag against chlorides, investigated by comparing chloride profiles after migration and diffusion, Mater. Struct. 46 (1) (2013) 89–103.
[38] O.R. Ogirigbo, L. Black, Chloride binding and diffusion in slag blends: Influence of slag composition and temperature, Constr. Build. Mater. 149 (2017) 816–825.
[39] S. Sui, F. Georget, H. Maraghechi, W. Sun, K. Scrivener, Towards a generic approach to durability: Factors affecting chloride transport in binary and ternary cementitious materials, Cem. Concr. Res. 124 (2019) 105783.
[40] A. Arora, G. Sant, N. Neithalath, Ternary blends containing slag and interground/blended limestone: Hydration, strength, and pore structure, Constr. Build. Mater. 102 (2016) 113–124.
[41] S. Adu-Amankwah, M. Zajac, J. Skoček, J. Němeček, M.B. Haha, L. Black, Combined influence of carbonation and leaching on freeze-thaw resistance of limestone ternary cement concrete, Constr. Build. Mater. 307 (2021) 125087.
[42] W. Arnold, P. Astel, T. Forman, M.P. Drewniok, The efficient use of GGBS in reducing global emissions, Institution of Structural Engineers, United Kingdom, 2023.
[43] BS 7979, Specification for limestone fines for use with Portland cement, BSI Standards Limited, London, 2016.
[44] BS EN 206:2013+A2. Concrete — Specification, performance, production and conformity, British Standards Institute, London, 2021.
[45] BS EN 12390-2, Testing hardened concrete. Making and curing specimens for strength tests, British Standards Institution, London, 2019.
[46] BS EN 12350-2, Testing fresh concrete. Slump-test, British Standards Institution, London, 2019.
[47] BS EN 12350-5, Testing Fresh Concrete. Flow Table Test, British Standard Institute, London, 2019.
[48] BS EN 12350-6, Testing fresh concrete. Density, British Standards Institution, London, 2019.
[49] BS EN 12390-3, Testing Hardened Concrete: Compressive Strength of Test Specimens, British Standard Institute, London, UK, 2019.
[50] BS EN 12390-5, Testing Hardened Concrete. Flexural Strength of Test Specimens, British Standard Institution, London, 2019.
[51] ASTM C469/C469M, Standard Test Method for Static Modulus of Elasticity and Poisson's Ratio of Concrete in Compression, ASTM International, West Conshohocken, PA, 2022.
[52] BS EN 12504-4, Testing concrete. Determination of ultrasonic pulse velocity, British Standards Institution, London, 2021.
[53] BS EN 12390-7, Testing Hardened Concrete: Density of Hardened Concrete, British Standards Institution, 2019.
[54] ASTM C-597, Standard test method for pulse velocity through concrete, American Society for Testing and Materials, West Conshohocken, PA, USA, 2002.
[55] M. Anson, K. Newman, The effect of mix proportions and method of testing on Poisson's ratio for mortars and concretes, Mag. Concr. Res. 18 (56) (1966) 115–130.
[56] ASTM C 1760, Stand. Test. Method Bulk. Electr. Conduct. hardened Concr. (2012).
[57] Nordtest NTBuild 492, Concrete, Mortar, Cement Based Repair Materials: Chloride Migration Coefficient from Non-steady State Migration Experiments, 1999.
[58] BS EN 13057, Products and systems for the protection and repair of concrete structures, Test. Methods Determ. Resist. Capill. Absorpt. (2002).
[59] BS 1881-208, Recommendations for the determination of the initial surface absorption of concrete, British Standards Institution, London, 1996.
[60] A. Djerbi Tegguer, S. Bonnet, A. Khelidj, V. Baroghel-Bouny, Effect of uniaxial compressive loading on gas permeability and chloride diffusion coefficient of concrete and their relationship, Cem. Concr. Res. 52 (2013) 131–139.
[61] I. Ismail, S.A. Bernal, J.L. Provis, R. San Nicolas, D.G. Brice, A.R. Kilcullen, S. Hamdan, J.S.J. van Deventer, Influence of fly ash on the water and chloride permeability of alkali-activated slag mortars and concretes, Constr. Build. Mater. 48 (2013) 1187–1201.
[62] C. White, J.M. Lees, Effective utilisation of slag in concrete: insights into fresh-state performance retention, in: J.A.O. Barros, V.M.C.F. Cunha, H.S. Sousa, J.C. Matos, J. M. Sena-Cruz (Eds.), 4th fib International Conference on Concrete Sustainability (ICCS2024). ICCS 2024. Lecture Notes in Civil Engineering 573, Springer, Cham, 2025.
[63] S. Blotevogel, A. Ehrenberg, L. Steger, L. Doussang, J. Kaknics, C. Patapy, M. Cyr, Ability of the R^3 test to evaluate differences in early age reactivity of 16 industrial ground granulated blast furnace slags (GGBS), Cem. Concr. Res. 130 (2020) 105998.
[64] M.I.A. Khokhar, E. Rozière, P. Turcry, F. Grondin, A. Loukili, Mix design of concrete with high content of mineral additions: Optimisation to improve early age strength, Cem. Concr. Compos. 32 (5) (2010) 377–385.
[65] A. Darquennes, E. Roziere, M.I.A. Khokhar, P. Turcry, A. Loukili, F. Grondin, Long-term deformations and cracking risk of concrete with high content of mineral additions, Mater. Struct. 45 (11) (2012) 1705–1716.
[66] ACI 209R-92, Prediction of creep, shrinkage, and temperature effects in concrete structures, Acids Man. Concr. Pract. Part 1 Mater. Gen. Prop. Concr. 1994 (2004).
[67] J.M. Khatib, J.J. Hibbert, Selected engineering properties of concrete incorporating slag and metakaolin, Constr. Build. Mater. 19 (6) (2005) 460–472.
[68] P. Duan, Z. Shui, W. Chen, C. Shen, Enhancing microstructure and durability of concrete from ground granulated blast furnace slag and metakaolin as cement replacement materials, J. Mater. Res. Technol. 2 (1) (2013) 52–59.
[69] K.L. Scrivener, A.K. Crumbie, P. Laugesen, The interfacial transition zone (ITZ) between cement paste and aggregate in concrete, Interface Sci. 12 (4) (2004) 411–421.
[70] Building Code Requirements for Structural Concrete (ACI 318-19), American Concrete Institute, Farmington Hills, MI 48331, 2019.
[71] CSA A23, Design of Concrete Structures, Canadian Standard Association, Mississauga, ON, Canada, 2004, pp. 3–04.
[72] NZS-3101: Concrete structures standard—The design of concrete structures, Standards New Zealand, NZS Wellington, New Zealand, 2006.
[73] L. Taerwe, S. Matthys, Fib model code for concrete structures 2010, Ernst & Sohn, Wiley, 2013.
[74] BS EN 1992-1-1, Eurocode 2: Design of concrete structures, British Standard Institute, London, 2023.
[75] M. Shariq, J. Prasad, A. Masood, Studies in ultrasonic pulse velocity of concrete containing GGBFS, Constr. Build. Mater. 40 (2013) 944–950.

[76] Y. Zhou, J. Gao, Z. Sun, W. Qu, A fundamental study on compressive strength, static and dynamic elastic moduli of young concrete, Constr. Build. Mater. 98 (2015) 137–145.
[77] M. Bouasker, N.E.H. Khalifa, P. Mounanga, N. Ben Kahla, Early-age deformation and autogenous cracking risk of slag–limestone filler-cement blended binders, Constr. Build. Mater. 55 (2014) 158–167.
[78] K. Wu, H. Shi, L. Xu, G. Ye, G. De Schutter, Microstructural characterization of ITZ in blended cement concretes and its relation to transport properties, Cem. Concr. Res. 79 (2016) 243–256.
[79] J.J. Chen, A.K.H. Kwan, Y. Jiang, Adding limestone fines as cement paste replacement to reduce water permeability and sorptivity of concrete, Constr. Build. Mater. 56 (2014) 87–93.
[80] V.. Baroghel-Bouny, Which toolkit for durability evaluation as regards chloride ingress into concrete? Part II: Development of a performance approach based on durability indicators and monitoring parameters, pp. 137-163.
[81] K.Y. Yeau, E.K. Kim, An experimental study on corrosion resistance of concrete with ground granulate blast-furnace slag, Cem. Concr. Res. 35 (7) (2005) 1391–1399.
[82] Y. Dhandapani, M. Santhanam, Investigation on the microstructure-related characteristics to elucidate performance of composite cement with limestone-calcined clay combination, Cem. Concr. Res. 129 (2020) 105959.
[83] P. Rodulfo, B. Wang, R. Gupta, L. Sharma, P. Mukhopadhyaya, Relationship between electrical Conductivity, Half cell Potential, Linear polarization resistance and Macrocell current of cementitious repair materials, Constr. Build. Mater. 401 (2023) 132733.
[84] U.M. Angst, Steel corrosion in concrete – Achilles' heel for sustainable concrete? Cem. Concr. Res. 172 (2023) 107239.
[85] W. Wilson, F. Georget, K.L. scrivener, Towards a two-step assessment of the chloride ingress behaviour of new cementitious binders, Cem. Concr. Res. 184 (2024) 107594.
[86] J.E. Vigor, D.P. Prentice, X. Xiao, S.A. Bernal, J.L. Provis, The pore structure and water absorption in Portland/slag blended hardened cement paste determined by synchrotron X-ray microtomography and neutron radiography, RSC Adv. 14 (7) (2024) 4389–4405.
[87] W. Wilson, F. Georget, K.L. Scrivener, Unravelling chloride transport/microstructure relationships for blended-cement pastes with the mini-migration method, Cem. Concr. Res. 140 (2021) 106264.
[88] P. Ghosh, Q. Tran, Correlation between bulk and surface resistivity of concrete, Int. J. Concr. Struct. Mater. 9 (1) (2015) 119–132.
[89] G. Jagan, C. Gary, Resistivity tests for concrete - Recent field experience, ACI Maters J 113 (4) (2016).
[90] L. Tang, L.-O. Nilsson, P.M. Basheer. Resistance of concrete to chloride ingress: Testing and modelling, CRC Press, Taylor and Francis Group, 2012.
[91] M. Saillio, V. Baroghel-Bouny, F.J.C. Barberon, B. Materials, Chloride binding in sound and carbonated cementitious materials with various types of binder, Constr. Build. Mater. 68 (2014) 82–91.
[92] Y. Dhandapani, M. Santhanam, On the correlations between different chloride transport parameters and their role in service life estimation, Sustain. Resilient Infrastruct. 8 (2022) 240–255.
[93] V. Baroghel-Bouny, K. Kinomura, M. Thiery, S. Moscardelli, Easy assessment of durability indicators for service life prediction or quality control of concretes with high volumes of supplementary cementitious materials, Cem. Concr. Compos. 33 (8) (2011) 832–847.